Hyperboloid Rocket Engine HypE

EFFICIENCY ADVANCEMENTS IN NOVEL APPROACHES FOR LIQUID HIGH PERFORMANCE ROCKET THRUST CHAMBERS

M. Ortelt,[1,*] S. Michaelides,[2] G. Herdrich,[3] & H. Seiler[1]

[1]German Aerospace Center, Pfaffenwaldring 38-40, D-70569 Stuttgart, Germany, E-Mail: markus.ortelt@dlr.de, helge.seiler@dlr.de

[2]Philopimenos 16, Limassol, 3075 Cyprus, E-Mail: mstels@web.de

[3]University of Stuttgart, Institute of Space Systems, Pfaffenwaldring 29, D-70569 Stuttgart, Germany, E-Mail: herdrich@irs.uni-stuttgart.de

Abstract

DLRs so-called cone injector design, a new injection method adjusted initially to the function of transpiration cooled ceramic rocket thrust chambers became of high interest in the recent years, with regard to improved spray forming, ignition and combustion, Derived from the typical hyperboloid injection spray shape coming from the cone injector design, the idea of a continuous hyperboloid sub-sonic inner combustion chamber contour arose. More homogeneous boundary layers particularly in the thermally critical near-throat-zone reduce surface temperatures. Additionally the inclusion of the chamber walls for the propellant injection using a specific dual-shell hyperboloid design promise the potential of a so-called injection cooling method leading to highly efficient and thermochemical safe combustion chamber operation. First screenings while performing CFD and combustion simulations promise improvements concerning thrust chamber efficiency accompanied by the increase of reliability and lifetime at low cost level.

KEY WORDS: *Ceramic rocket thrust chamber, combustion chamber contour, rocket propellant*

injection, rocket propellant combustion, I_{sp} improvement, high reliability, fatigue reduction, high lifetime.

1. INTRODUCTION

Within DLRs long-lasting development of transpiration cooled ceramic rocket thrust chamber assemblies (TCA, Greuel 2013, Haidn 2003, Hald 2005, Ortelt 2009, 2012, 2013, 2014, Herbertz 2012, Selzer 2012) for high performance application (Fig. 1, left), in a very early status, the use of the porous ceramic inner walls as a part of the injector had already been discussed intensively. To bring the inflow of the first propellant component, coming through the porous wall surfaces, into close contact with the second propellant component, coming from the traditional injector head, the typical combustion chamber geometry is not applicable for complete mixing and combustion. As a consequence the so-called cone-injector-head design (Fig. 1, right), which was primarily, tailored for the use of highly permeable CMC (Ceramic Matrix Composite) materials in an innovative low-fatigue injector head structure, found its additional advantage in a new

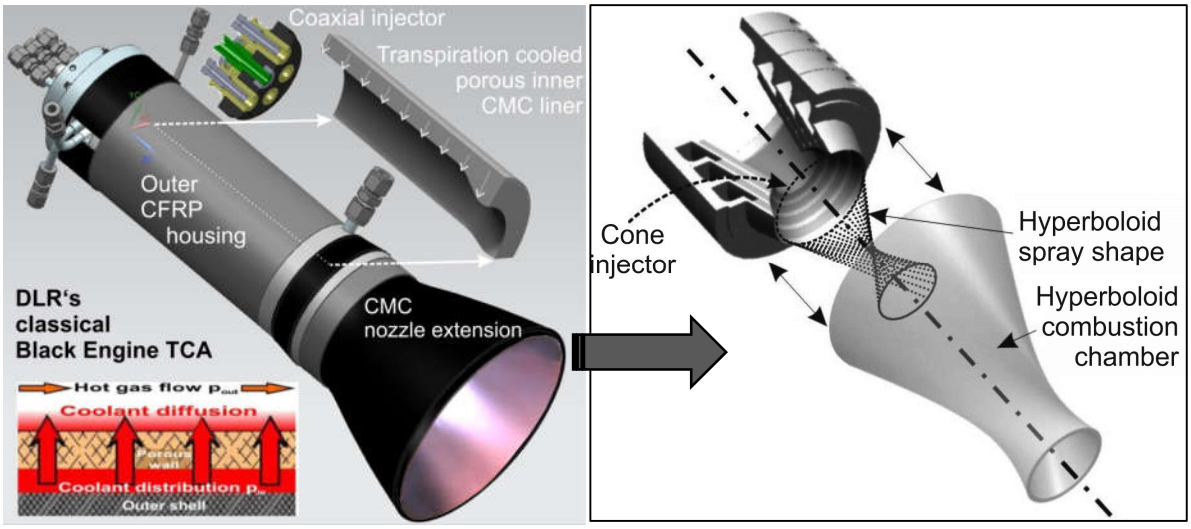

FIG. 1: Transition from classical design to combined cone injector and hyperboloid chamber.

cooling method, the so-called injection cooling. Herein the functions of injection and cooling will be combined, while the traditional inner wall contour changes from the conventional cylinder-Laval-nozzle-shape to a mathematical one-shell-hyperboloid-shape (Fig. 2, red contour line, longitudinal half-sections), (Ortelt 2017, Schleutker 2014), which is aligned on the injector side to the cone-section-outlet of the new injector head To bring the two propellant components in adequate contact for sufficient mixing capability a tapering inner core body (blue contour line), showing the shape of a two-shell-hyperboloid will be inserted attached to the injector head faceplate. Consequently a cramped ring-shaped interior mixing and combustion zone with higher contact surface ratio arises compared to the classical contour.

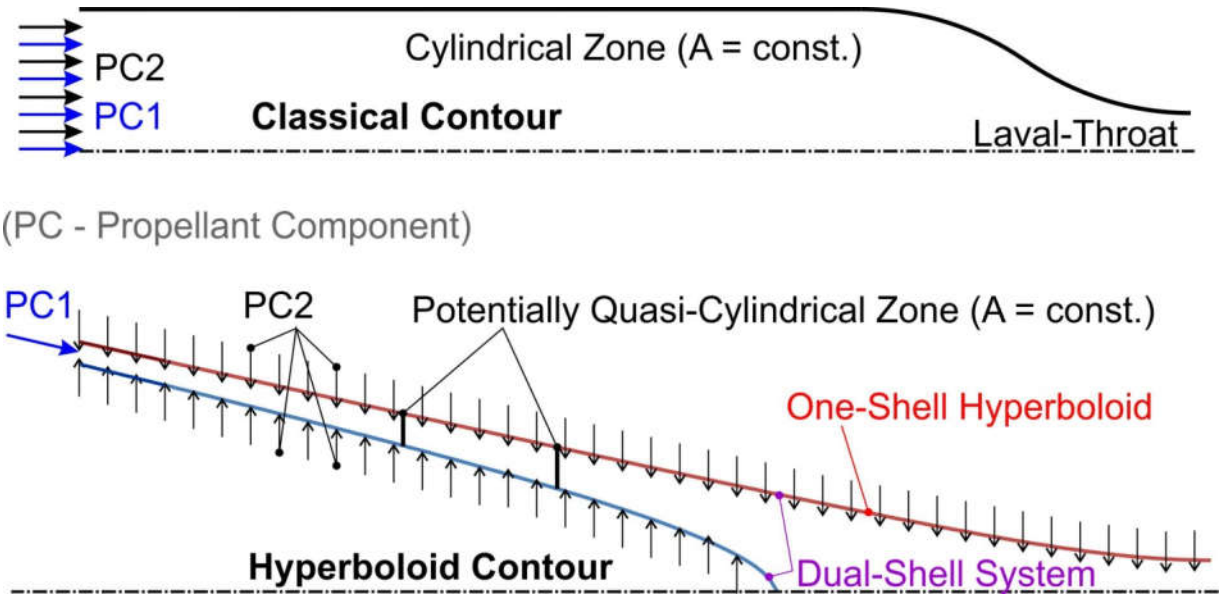

FIG. 2: New combustion chamber design approach using dual-shell hyperboloid wall contours.

The geometry described before promises the successful injection cooling method proven by first numerical screenings on subscale level. The efficiency of up-scaled designs depends on further improvements in the mixing zone. The final goal is the improvement of reliability and

operational safety caused by the inherently higher blow rate at the inner combustion chamber wall surfaces as well as the increase of the overall efficiency at I_{sp} optimal operation conditions generated by the exclusion of pressure loss, traditionally caused by separated cooling systems.

2. BASIC IDEAS OF THE NEW DESIGN APPROACH

The structure principle of the cone injector design (Ortelt 2010) consists of a stack of single hollow-conical injector elements, which are fit together like a stack of paper cups (Fig. 1, top-right). It is a rotation symmetric design of principally different and alternating "cup" elements for the injection of fuel, oxidant and the separation of both functions. In the current design the oxidant will be injected through hollow-conical elements containing a well-defined system of very thin skew channels (Fig. 3). Such elements can be manufactured of CMC materials or 3D-printed metal parts. The fuel will be injected through intermediate ring-shaped gaps, which can also have texturized contours.

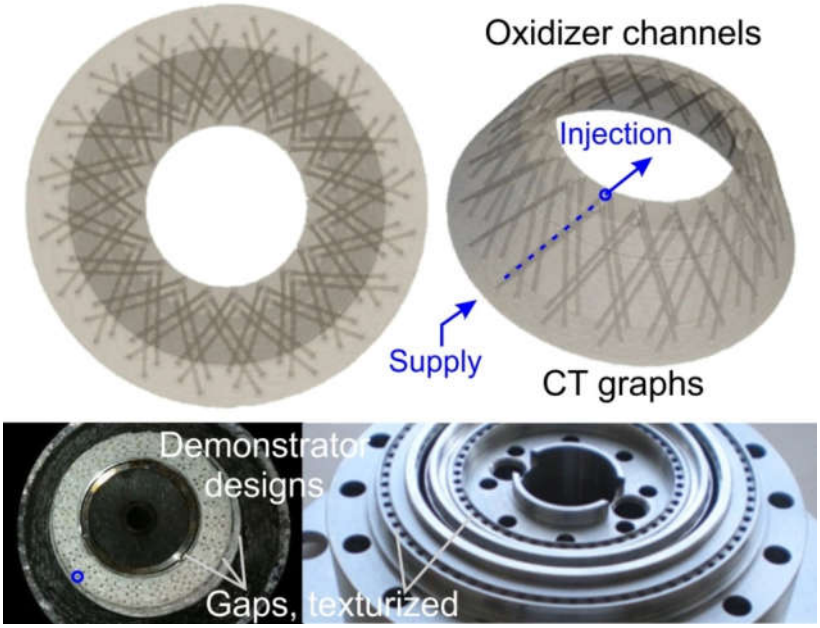

FIG. 3: Injector-inherent channel and gap arrays of the current demonstrator designs, 50 mm-TCA (left), gas generator (right).

The principle of the new dual-shell hyperboloid design approach (Fig. 1 and 4) shows the following specifics: For a better comparison to the classical contour and to prevent geometrically triggered flow acceleration in the combustion zone in principle the inner core body follows the contour of an adjusted two-shell hyperboloid line, so that the cross section area in the quasi-cylindrical combustion chamber zone remains constant.

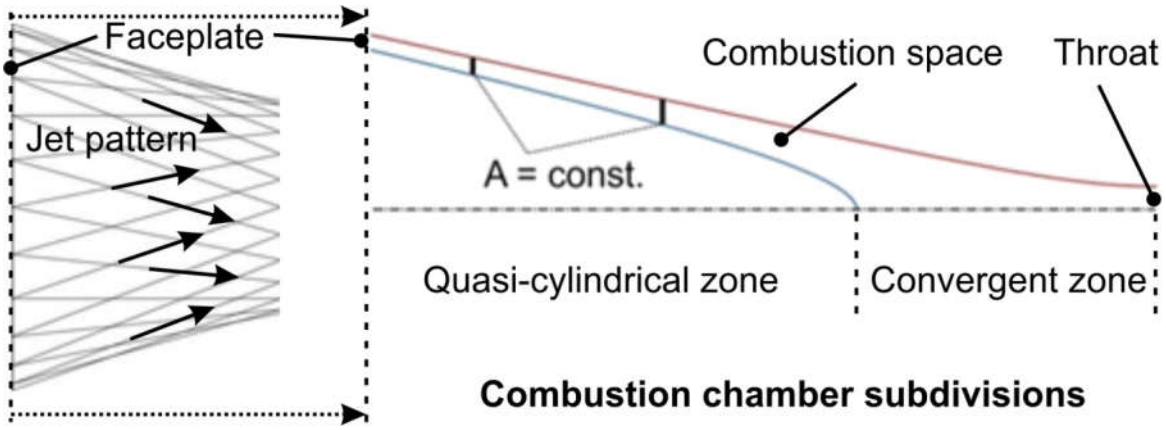

FIG. 4: Design specifics of the dual-shell hyperboloid geometry.

In such a combustion chamber contour design the (quasi-) cylindrical zone goes over automatically into the convergent zone without any change of curve direction of the contour lines. That leads to more homogeneous flow (Schleutker 2014) along the wall contours (Fig. 5, viscosity plot), compared to classical Laval design, particularly in the boundary layer close to the nozzle throat.

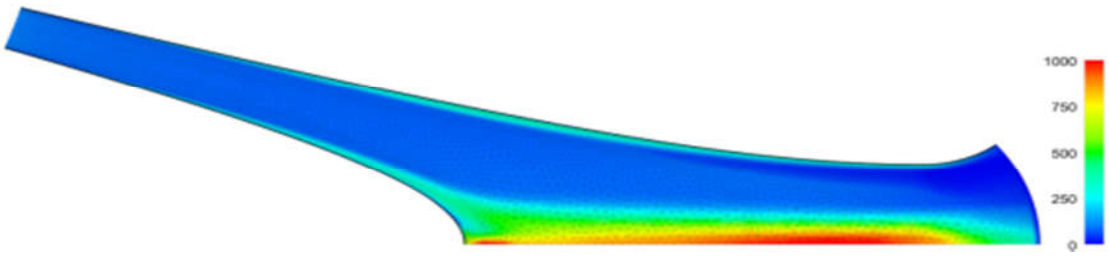

FIG. 5: Viscosity plot in the dual-shell hyperboloid hot gas flow, showing turbulence free

homogeneous boundary layers (half-section displayed).

The increase of homogeneity in the boundary layers results in significantly reduced heat load peaks, especially in the thermally critical Laval-throat region (Fig. 6), which leads to stress reduction of the chamber structure and a final increase of structural reliability.

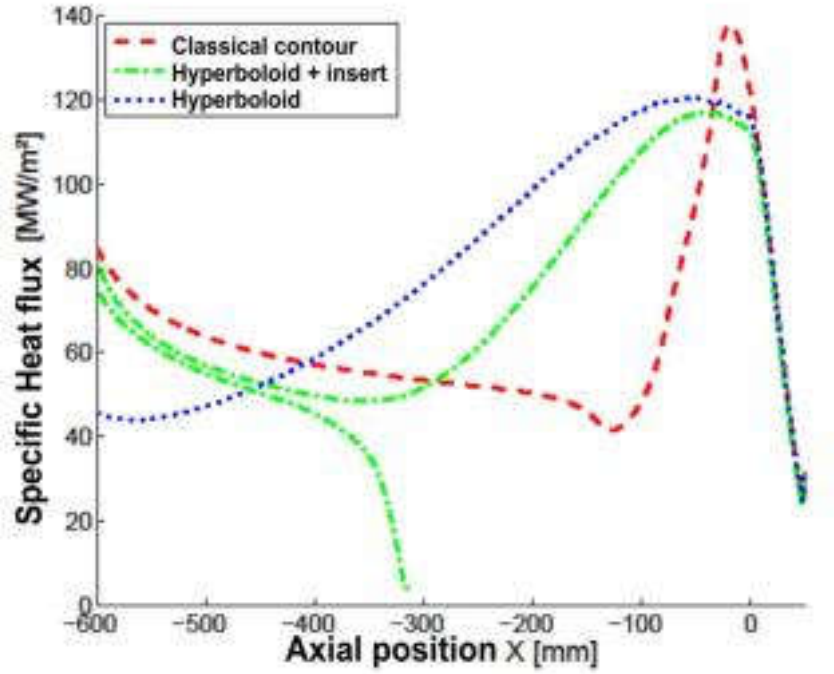

FIG. 6: Reduction of heat load peak, using the dual-shell hyperboloid design.

For the investigation of the new design approach a multifunctional demonstrator has been manufactured (Fig. 7), which one and the same shall be operated on the one hand in a full-scale gas-generator application at low mixture ratio and on the other hand in a sub-scale main-chamber application at higher mixture ratio, using liquid oxygen and liquid methane as bi-propellant components. The chamber pressures will range around 60 bar. It will be expected, that the exit temperature distribution in the gas generator application will be adequately homogeneous (Fig.

10) for safe operation of the turbine blades without any additional arrangements, like distributor grids. That aspect follows again the general design motivation for system-simplified structure concepts (Seiler 2017).

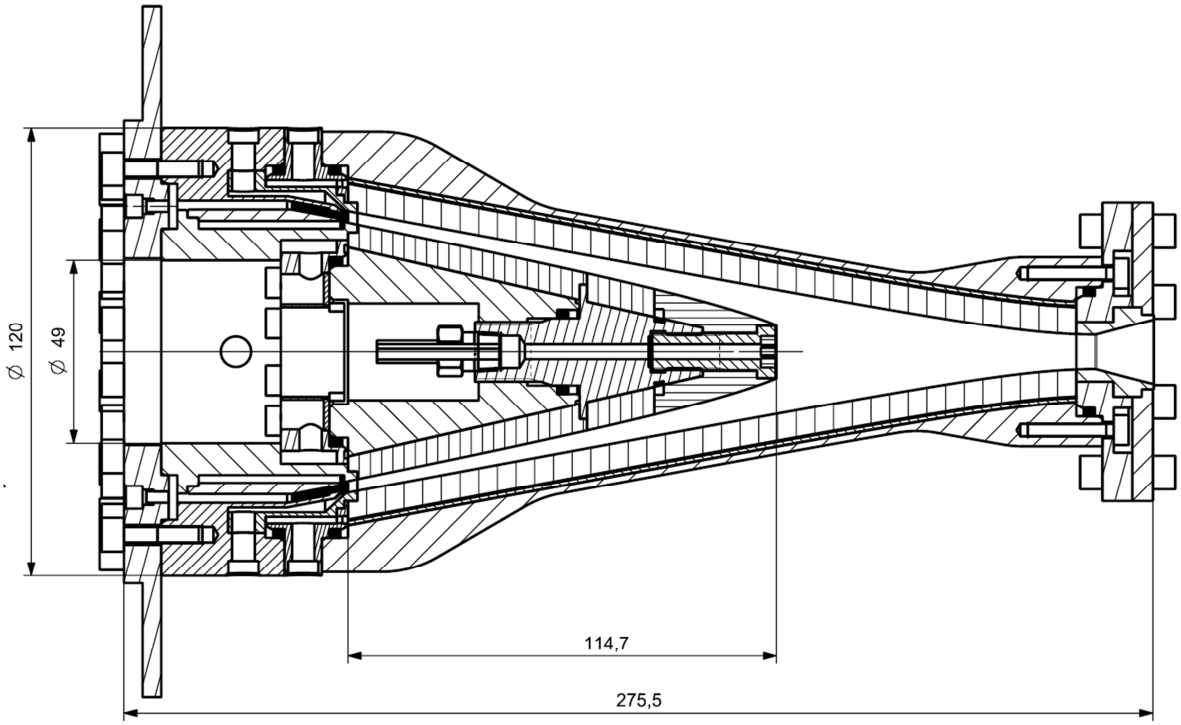

FIG. 7: Dual-shell hyperboloid demonstrator for full-scale gas-generator and sub-scale main chamber application.

3. FIRST CFD SCREENING

In a first set of computed fluid dynamics simulation, applying Ansys-CFX, six geometric configurations have been investigated, focusing primarily the gas generator application. Figure 8 shows firstly the geometric variation, whereas the qualitative evaluation will show the method of how to find the geometric optimum. Case 5 of 6 fits the functional request best and will be discussed in the following section. Figure 8 additionally shows highlighted the model cut-out of

geometry case No. 5. The definition of the chamber geometry in principle bases on the operational boundary conditions given from WEPA-Technologies (Weuta 2016), the producer of the corresponding turbo pump system, and, the creator of the turbine inflow conditions respectively.

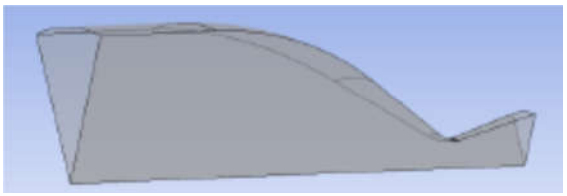

Case No. 1

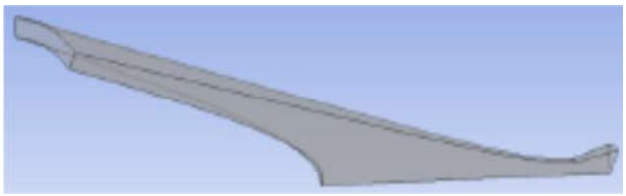

Case No. 2

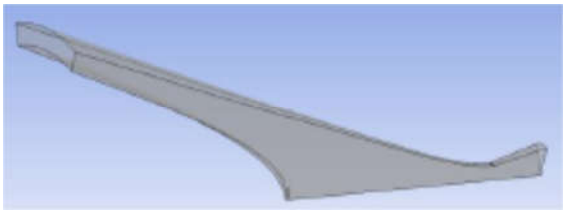

Case No. 3

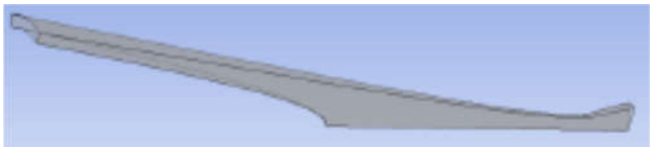

Case No. 4

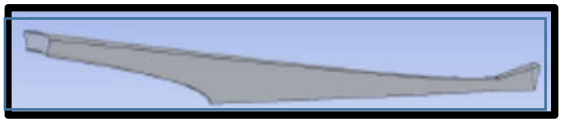

Case No. 5

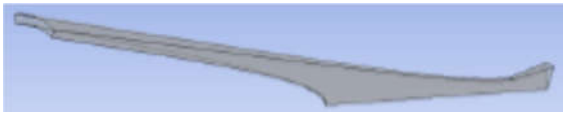

Case No. 6

FIG. 8: Geometric variation of the gas generator chamber design.

The operational chamber pressure amounts to 54 bar, the overall mass flow to 400 g/s, static exit pressure and velocity to 3 bar and 1200 m/s. The final geometry, contraction 10.64 and mixture ratio 0.27 have been calculated by RPA. The one –shell hyperboloid geometry generally follows Eq. (1), the two-shell hyperboloid Eq. (2).

$$\frac{y^2}{b^2}+\frac{z^2}{c^2}-\frac{x^2}{a^2}=1 \quad \rightarrow \quad \frac{y^2}{b^2}-\frac{x^2}{a^2}=1\ (rotational\ symmetry) \tag{1}$$

$$\frac{y^2}{b^2}+\frac{z^2}{c^2}-\frac{x^2}{a^2}=-1 \quad \rightarrow \quad \frac{y^2}{b^2}-\frac{x^2}{a^2}=-1\ (rotational\ symmetry) \tag{2}$$

Consequently the continuous contour lines inside the sub-sonic combustion chamber section can be described by one equation respectively.

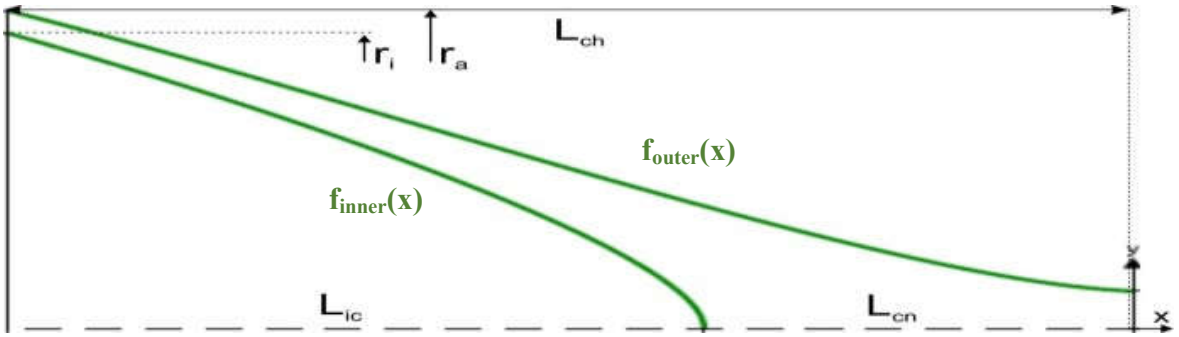

FIG. 9: Dimensions of the dual-shell hyperboloid gas generator chamber.

The dimensions of the chamber geometry are given in figure 9. Important are the relations between the diameter and length magnitudes, from which the characteristic chamber length, Eg. (3), will be derived. The chamber volume can be derived from the volumes of the rotational bodies by integration of the contour lines and afterwards by subtraction of the outer and inner body, Eqs. (4) and (5).

$$L^* = \frac{V_{ch}}{A_t} \tag{3}$$

$$V_{ch} = \pi \cdot \int_{x_0}^{L_{ch}} \left(f_{outer}(x)\right)^2 dx - \pi \cdot \int_{x_0}^{L_{ic}} \left(f_{inner}(x)\right)^2 dx \tag{4}$$

$$r(x=0) = \frac{b}{a} \cdot \sqrt{a^2 + 0^2} = b = r_t \tag{5}$$

The concrete dimension is r_a = 45 mm and the total chamber length is L_{ch} = 200 mm. The latter orients on the experience of the former technology research for the transpiration cooled CMC TCA (Seiler 2017, Michaelides 2017) where the characteristic chamber length amounted to 1.76 m. Slightly following the tendency towards lower L* as seen in full-scale chambers, but also using the latest research, the finally used value was approximately 1.6. m. Table 1 shows the relevant chamber geometry.

TABLE 1. Relevant dimensions of the gas generator chamber

L_{ch} (m)	L_{ic} (m)	L_{cn} (m)	L^* (m)	r_t (mm)	a (mm)	ε (-)
200	**123.61**	**76.39**	**1.637**	**4.605**	**24. 6**	**10.64**

Propellant component PC1 (oxidant) amounted to 0.085 kg/s. The inner fuel injection (PC2 inner) amounted to 0.2 kg/s and PC2 outer to 0.115 kg/s. The coefficient of heat transfer amounted to α = 4285 W/m^2 K, and the ambient temperature was defined to be 300 K. Figure 10 shows the distribution of temperature, pressure and exit velocity in the geometric configuration with the best operational fit (case 5). Comparing the shapes of the six different cases one interesting property found is the fact, that the geometric optimum quotient of L_{ic} an L_{cn} lies in the golden section (Φ = 1.618) in case 5. Whether this can be a coincidence shall be investigated in future development. Of-course the golden section would be a very interesting design guide value whether it could be proven in conjunction with this design approach.

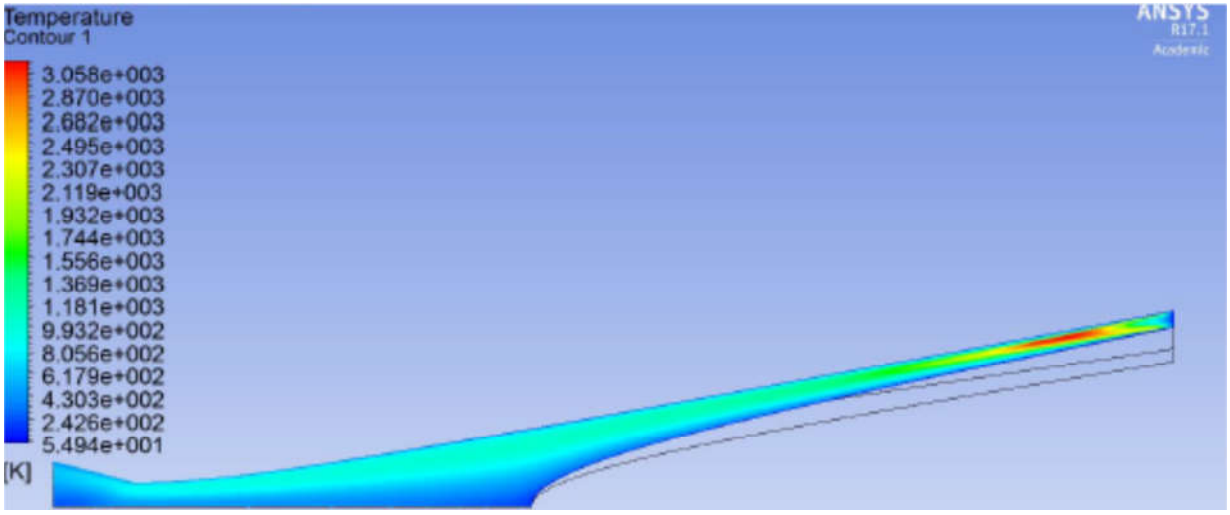

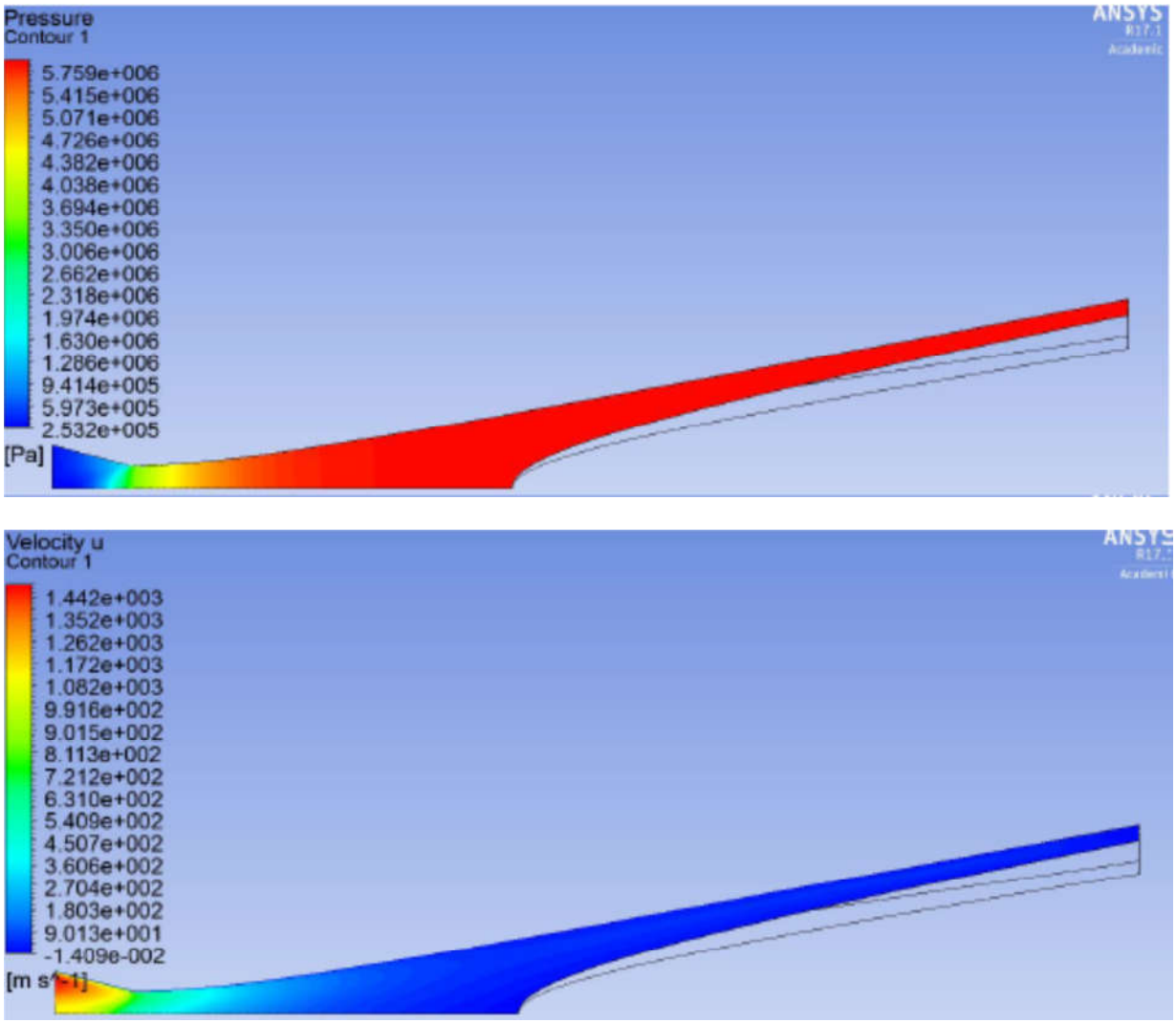

FIG. 10: Distribution of temperature (top), pressure (middle) and exit velocity (bottom) in a representative gas-generator application.

4. FIRST NUMERICAL COMBUSTION SCREENING

For the evaluation of the combustion principle in this specific application approach the processes of propellant injection, mixing and combustion modelling have been screened preliminarily by the use of simple standard methods and tools, just to get a first impression, how the way for further investigation can look (Michaelides 2017).

4.1 Fuel injection

As mentioned before, one of the major advantages of the hyperboloid ceramic rocket thrust chamber is the possibility of the injection-cooling and the so achieved non-destructive thermochemical-stress for the chamber-material. The resulting new fuel-injection-configuration was numerical investigated, to give an idea of the phenomena during the dispersion- and combustion-processes and how the injection-elements should be dimensioned and placed in the faceplate.

The injection-cooling approach makes use of the porous ceramic chamber walls. The complete cryogenic fuel-flow is being injected over the channel '1' and the distributer '4', through the porous ceramic walls '2,3' and the oxidant is being injected through injection-channels in the cone-injector '5'. (Fig. 3, top, Fig. 11)

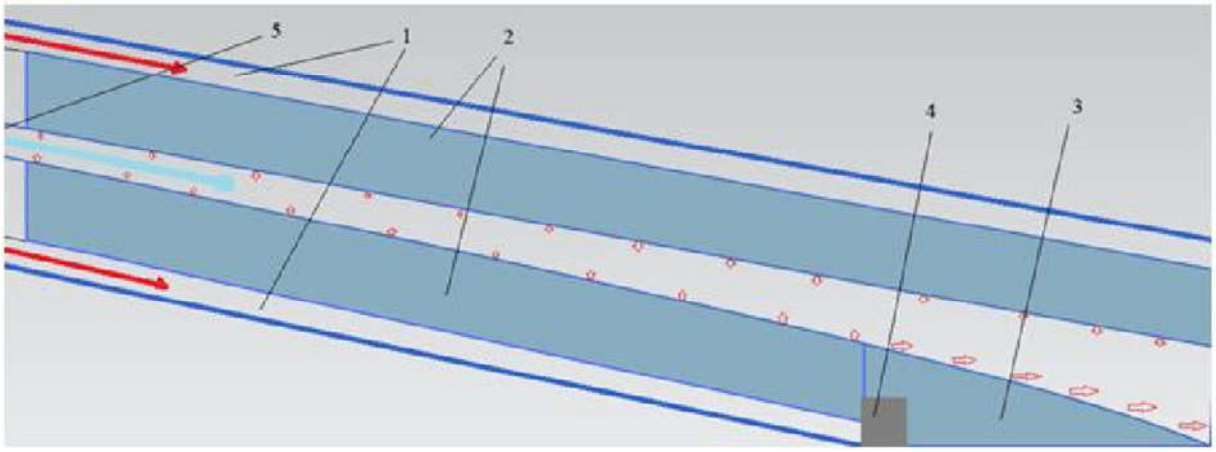

FIG. 11: Hyperboloid-chamber injection-cooling configuration.

As shown in figure 11 the inflow at segment '3' is created more in axial direction to provide additional cooling for the screw fixing the inner hyperboloid body (Fig. 7), where extreme heat load is being expected. As the chamber is driven fuel-rich, this injection configuration is believed

to provide full combustion of the reactive fluids, considering I_{sp}-optimal mixing conditions, in addition to a sustain cooling of the chamber walls. Compared to completely separated wall cooling this method provides principally higher blow rate combined with the injection of the main fuel flow.

4.2 Characterizing the Spray

As a first step for the characterization of the spray the thermodynamic conditions at the injection were inspected. The following table 2 gives the thermodynamic properties of the injected fluids.

TABLE 2. Properties of reactants

Properties	**O2**	**CH4**
Pressure at critical point p_{crit}(MPa)	**5.04**	**4.6**
Temperature at critical point T_{crit}(K)	**154.6**	**190.6**

As the chamber is to be driven at higher pressure than the critical pressure of the injected oxygen-jet, the jet-properties were expected similar to the injection in supercritical atmosphere.

4.2.1 Injection into critical atmosphere

Fortunately, a number of experimental studies were made investigating the injection of liquids into supercritical atmosphere. The following figure 12 (left) shows the change of the appearance of the injected liquid at different pressures ($P_r = \frac{p}{p_{crit}}$). (Chehroudi, Davis, Talley 2002)

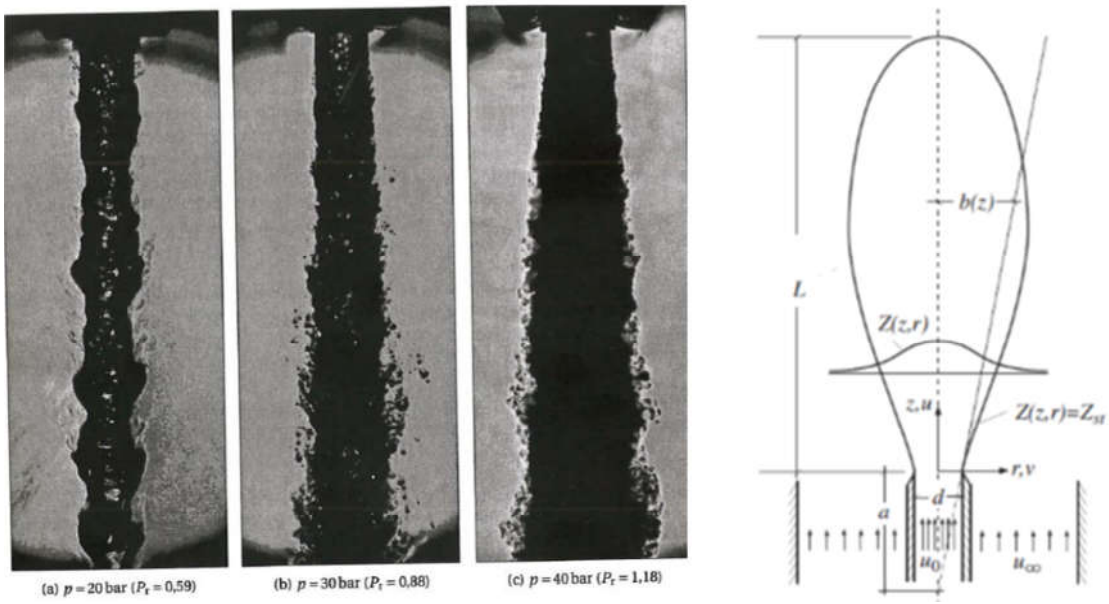

FIG. 12: Jet-appearance at different injection-pressures (left), diffusion-flame (right).

As the pressure gets supercritical the liquid jet stops dispersion and starts behaving like a gas jet without surface tension (Chehroudi, Davis, Talley 2002).

4.3 Mixing mechanism

As the gaseous-like oxygen-jet is injected into a gaseous-like methane-atmosphere, due to the very low radial methane velocity relatively to the oxygen-jet velocity, the combustion is expected to behave similar to turbulent diffusion-jet-flames (Fig. 12, right). Analytical models (Peters 2010) and experimental studies (Thring, Mewby 1953) were consulted for this type of combustion. The following two Eqs. (6) and (7) for the combustion-length are the result of the analytical model and the experimental researches. The equations are almost identical, except that the analytical Eq. (7) has instead of the injected fluids concentration, a in the combustion-theory often used property called mixture fraction Z (Peters 2010).

$$\frac{L}{d} = \frac{5{,}3}{Z_{st}} \left(\frac{\rho}{\rho_{st}}\right)^{\frac{1}{2}} \tag{6}$$

$$\frac{L_x}{d} = 5{,}3 \frac{c_0}{c_x} \left(\frac{\rho}{\rho_{st}}\right)^{\frac{1}{2}} \tag{7}$$

$d - Injection - hole\ diameter$ $\quad c_0, c_x - concentration\ at\ beginnning, at\ length\ x$

$L - Flamelength$ $\quad Z_{st} - Mixture\ fraction\ of\ stochiometric\ mixture$

$\rho, \rho_{st} - density\ of\ the\ injected\ jet, density\ of\ stochiometric\ mixture$

5. BASICS OF NUMERICAL COMBUSTION MODELLING

In addition to the in the computational fluid dynamics used conservative equations of mass, momentum, energy and turbulence model, the numerical combustion modeling requires conservative equation for the change of the reacting fluids concentrations. A number of approaches is available for modeling the combustion chemistry, in this section only the non-premixed combustion PDF (probability-density-function) approach that provides Ansys Fluent will be shortly presented (Michaelides 2017).

5.1 Transport equations for the mixing fraction

Under the assumption of equal diffusivities, the species equations can be reduced to a single equation for the mixture fraction Z. The reaction source terms in the species equations are cancelled (since elements are conserved in chemical reactions), and therefore Z is a conserved quantity. While the assumption of equal diffusivities is problematic for laminar flows, it is generally acceptable for turbulent flows where turbulent convection overwhelms

molecular diffusion. The Favre mean (density-averaged) mixture fraction Eq. (8) is

$$\frac{\partial}{\partial t}\left(\bar{\rho}\tilde{Z}\right) + \nabla \cdot \left(\bar{\rho}\vec{u}\tilde{Z}\right) = \nabla \cdot \left(\left(\frac{\lambda}{c_p} + \frac{\eta_t}{Pr_t}\right)\nabla\tilde{Z}\right) + S_m + S_{user} \quad (8)$$

where λ is the laminar heat thermal conductivity, c_p the specific heat capacity of the mixture, η_t and Pr_t the turbulent dynamic viscosity and Prandtl- number. The source term S_m is due solely to transfer of mass into the gas phase from liquid fuel droplets or reacting particles. S_{user} is any user-defined source term. In addition to solving the Favre mean mixture fraction, ANSYS Fluent solves a conservation equation for the mixture fraction variance, $\widetilde{Z''^2}$, Eq. (9)

$$\frac{\partial}{\partial t}\left(\bar{\rho}\widetilde{Z''^2}\right) + \nabla \cdot \left(\bar{\rho}\vec{u}\widetilde{Z''^2}\right) = \nabla \cdot \left(\left(\frac{\lambda}{c_p} + \frac{\eta_t}{Pr_t}\right)\nabla\widetilde{Z''^2}\right) + C_g\eta_t \cdot \left(\nabla\tilde{Z}\right)^2 - \frac{C_d\bar{\rho}\varepsilon}{k}\widetilde{Z''^2} + S_{user} \quad (9)$$

where $Z'' = Z - \tilde{Z}$. *The values of the constants are* $C_g = 2{,}86$ *and* $C_d = 2$. The mixture fraction variance is used in the closure model describing turbulence-chemistry interactions. A detailed description of the closure model that is used to describe turbulence-chemistry interaction in the non-premixed PDF-approach in ANSYS Fluent can be obtained from the ANSYS Fluent Theory Guide (ANSYS 2016).

6. COMBUSTION MODELLING WITH ANSYS FLUENT

This section will describe the steps during the combustion modeling of the injection-cooling-approach with ANSYS Fluent.

As shown in figure 11, there is a constant interaction between the hot-gas-stream in the chamber and the cooling-stream throw the ceramic walls. As this interaction rises the complexity of the numerical modeling, a common and very easy approach to handle this interaction at the DLR is to separate the hot-gas and the porous-wall domains, transfer and iterate the boundary conditions.(Michaelides 2016)

6.1 Hot-gas domain

The hot-gas domain was modeled as a 3D-segment (Fig. 15). Table 3 contains the defined boundary conditions.

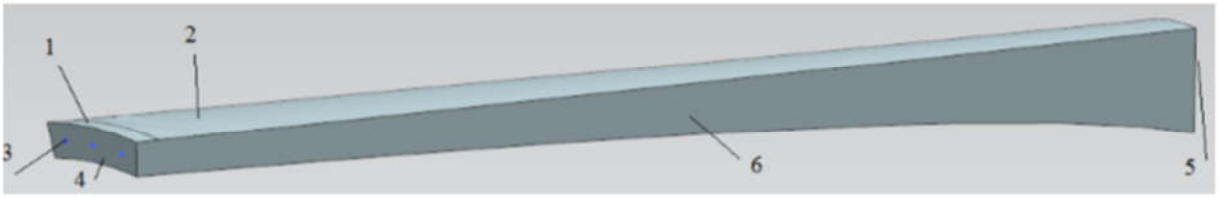

FIG. 13: 3D-segment of the hot-gas domain

As discussed in the sections 5 ANSYS Fluent solves the Navier-Stokes-Equations, the equations for the mixture fraction and its variance and the equations of the SST- turbulence-model that was used due to the conclusions that were made in [5], regarding to the interaction of hot-gas and porous-wall-stream. At the first iteration the inner wall temperature is assumed.

TABLE 3. Hot-gas boundary conditions

Segment	Type of boundary condition	Comment
1. Metallic wall	Adiabatic wall	-
2. Porous wall(upper, lower)	Wall,temperature, mass-source, momentum-source	As described in [5]
3. Oxygen injection holes	Inlet,oxygen-mass-flux, thermodynamic state	-
4. Faceplate	Adiabatic wall	-
5. Outlet	Outlet, chamber pressure	-
6. Model-side-segments	Periodic boundary condition	-

6.2 Porous wall domain

For a faster simulation the porous wall domains were modeled with a 2D-Mesh using the rotation-symmetrical approach ANSYS Fluent provides (Fig. 14).

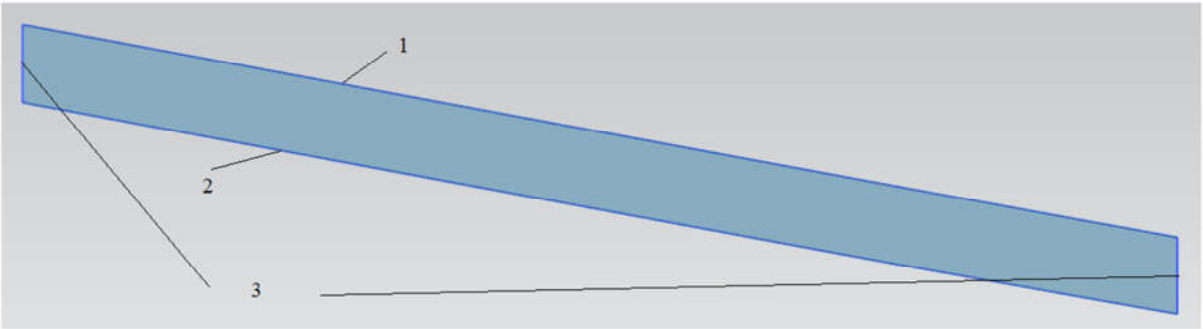

FIG. 14: Porous wall domain.

ANSYS Fluent solves for the porous domain the Darcy-Forchheimer-Equation and the energy-equation (ANSYS 2016). In the first iteration the heat-flux resulting from the first iteration of the hot-gas-domain-calculation is defined. The resulting temperature is then defined in the next iteration of the hot-gas-domain. The calculations were iterated until the boundaries matched.

7. STATUS-EVALUATION

This section describes the results of the combustion modeling regarding the efficiency of the transpiration-cooling-injection, the optimal injection-configuration and the former presented analytical models and experimental researches of the turbulent diffusion-flame (Michaelides 2017).

7.1 Influence of the thermodynamic state of the oxygen

From Eqs. (6) and (7) can be concluded that a lower density of the jet results in a lower flame-length and in a faster combustion process. Figure 15 shows the oxygen-mass-fraction at the inspected jet length at different inlet-temperatures. As expected from Eqs. (6) and (7) at a higher temperature and

so resulting lower density more oxygen has reacted at the end of the jet. Still, the injection-temperature should be hold at the critical point, as higher inlet-enthalpies result in a higher wall heat flux (Fig. 16).

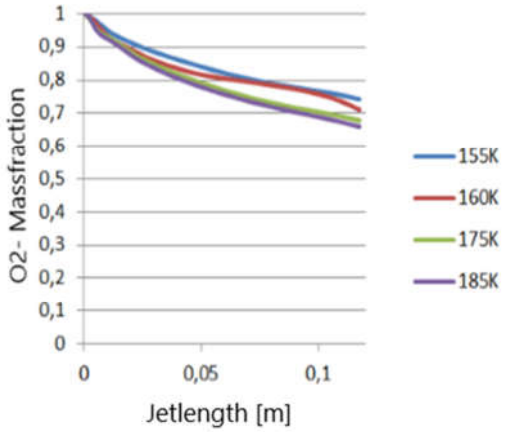

FIG. 15: O_2- Mass fraction at jet length.

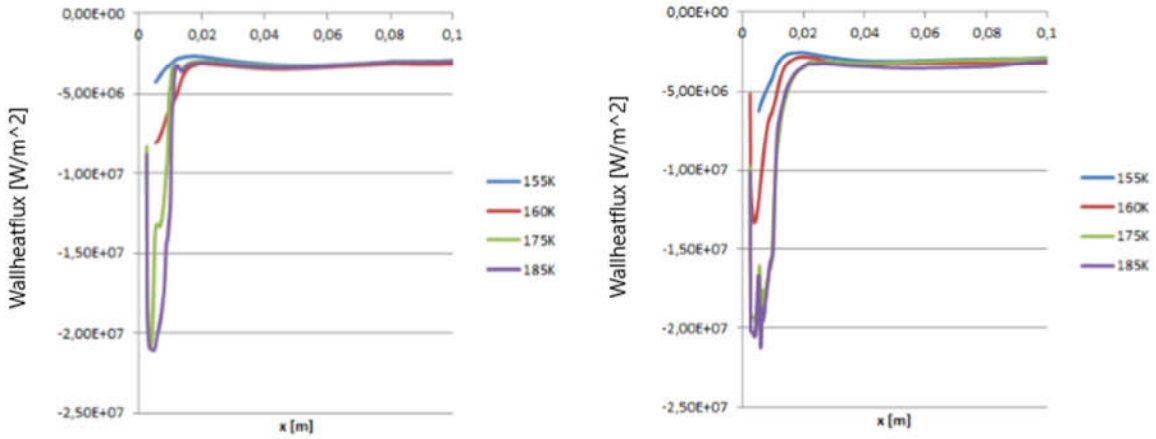

FIG. 16: Wall heat flux (left upper wall, right lower wall)

7.2 Influence of the wall injection

A number of wall-injection configurations were inspected varied by position and the intensity of the wall methane mass flow. The conclusion that was made is, that the for the complete combustion

needed methane mass flow should be injected over and until the end of the backflow vortex, so that enough methane is transported to the domain with the highest gradients.(Fig. 19, 20 and 21)

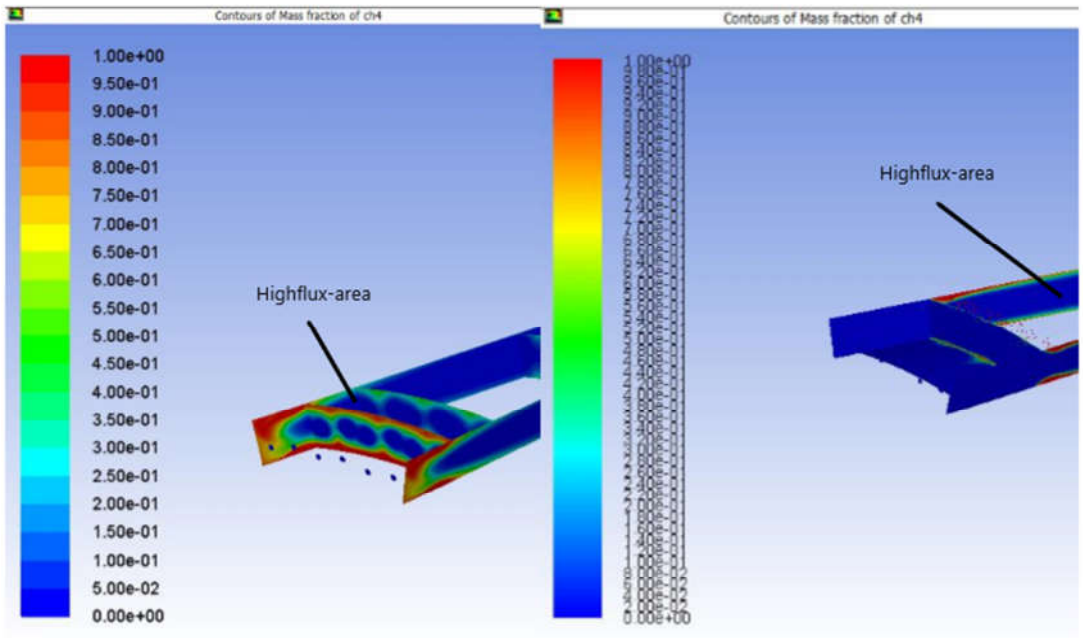

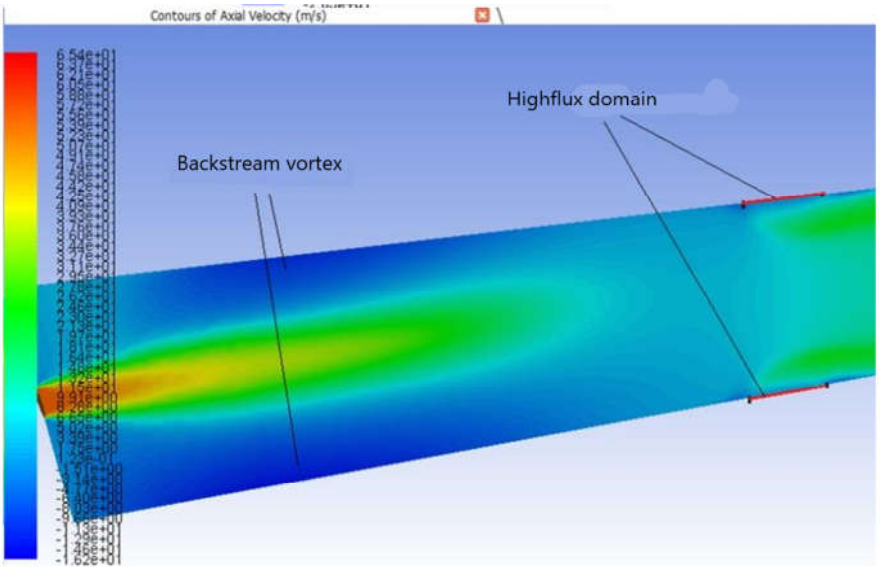

FIG. 17: Contours of mass fraction of methane at different high-flow-area position.

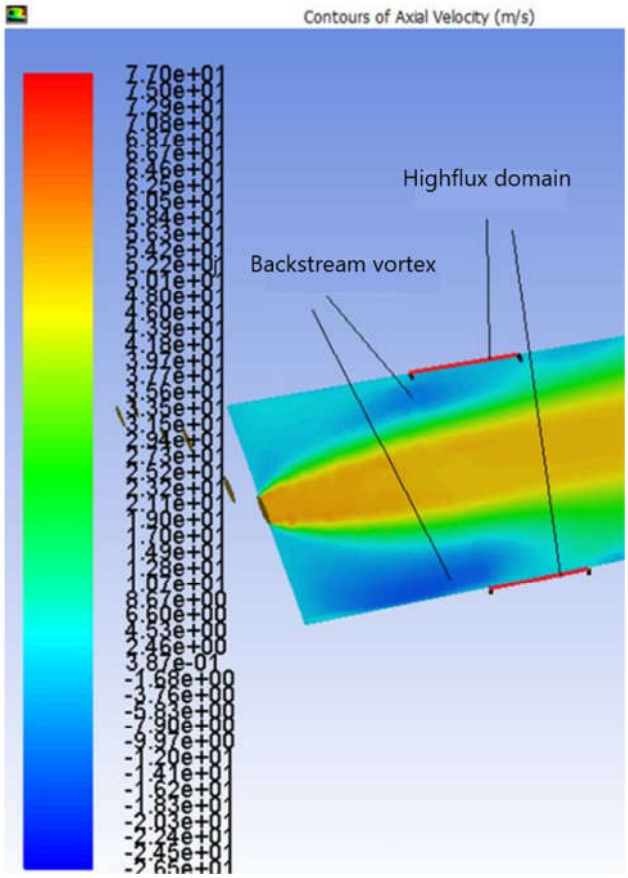

FIG. 18: Contours of axial velocity (m/s) at different high-flow domain position.

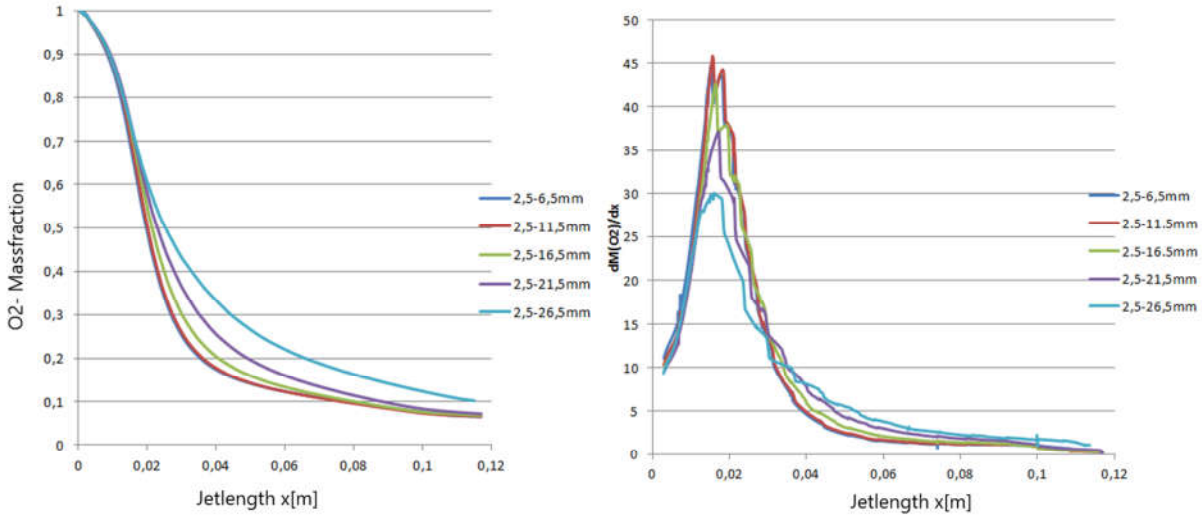

FIG. 19: Oxygen mass fraction and gradient at jet-length.

7.3 Influence of the injection-holes configuration

At last the influence of the injection-holes configuration was examined. As expected from Eqs. (6) and (7) a smaller jet-diameter results in a smaller flame-length and faster combustion.

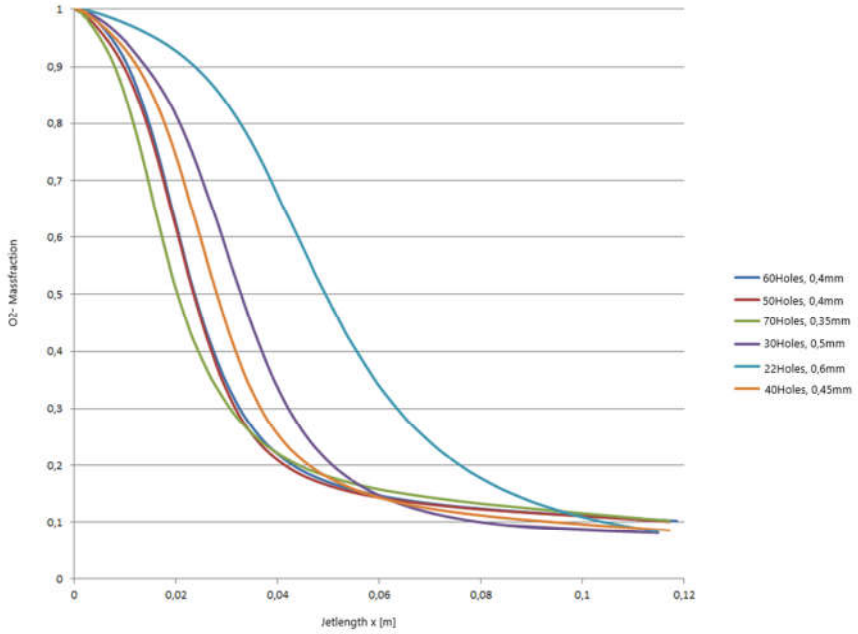

FIG. 20: Oxygen mass fraction over jet-length.

Although due to the fact, that smaller diameters resulted in more jets for the same mass flow, more jets would reach each other contours faster, diminish the contact surface between the two reacting fluids and slow the combustion process down.(Fig. 22 and 23).

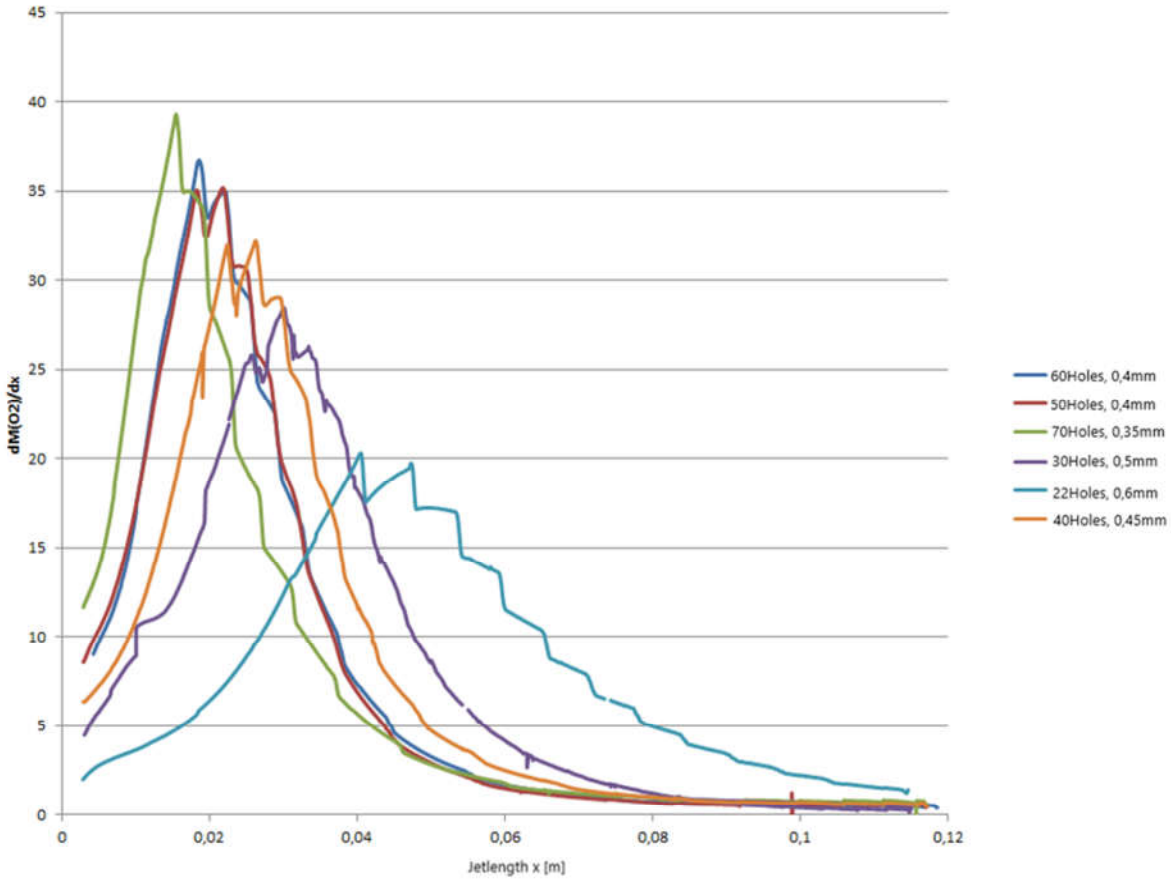

FIG. 21: Gradient over jet-length.

7.4 Match to analytical model

As the different contour-plots of the flame showed, the combustion behaved very similar to the assumed type of turbulent diffusion flame. Although, due to the fact that the flame in our case is in a limited chamber volume, one get the effect of the backstream vortex. The numerical calculated combustion process was compared to the analytical formula, showing a pretty good match to the assumption (Fig. 22).

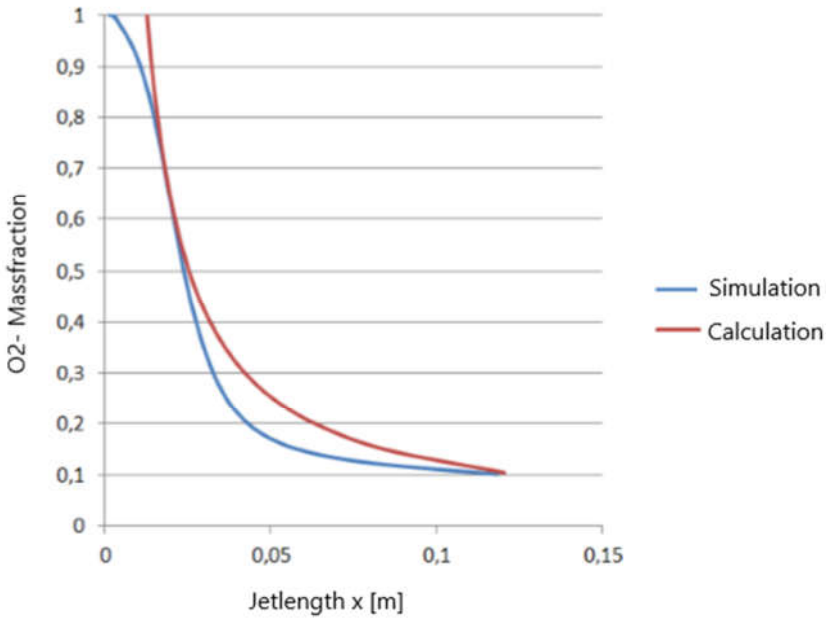

FIG. 22: Comparing the numerical and analytical results.

7.5 Efficiency of the injection-cooling

It was decided to extend the domain until the sonic point for the examined case with the best combustion performance, in order to prove the combustion and cooling Efficiency of the injection-cooling. Non-destructive wall conditions were achieved with only 5 % more methane for cooling. As the examined chamber is a subscale model, better cooling performance for the full scale chamber can be expected. Although, only 95% combustion could be achieved at the sonic point, where the major combustion is expected to be completed (Fig.23).

Regarding to the full-scale chamber it is expected, that the combustion slowing effect discussed in 7.3 will be even worse as the jet-amount relative to the chamber-flow-surface increases.

As a conclusion the injection-cooling-approach is still believed to be very promising, by combining it with the traditional coax-injection. The efficiency of the combined method has still to be numerically investigated.

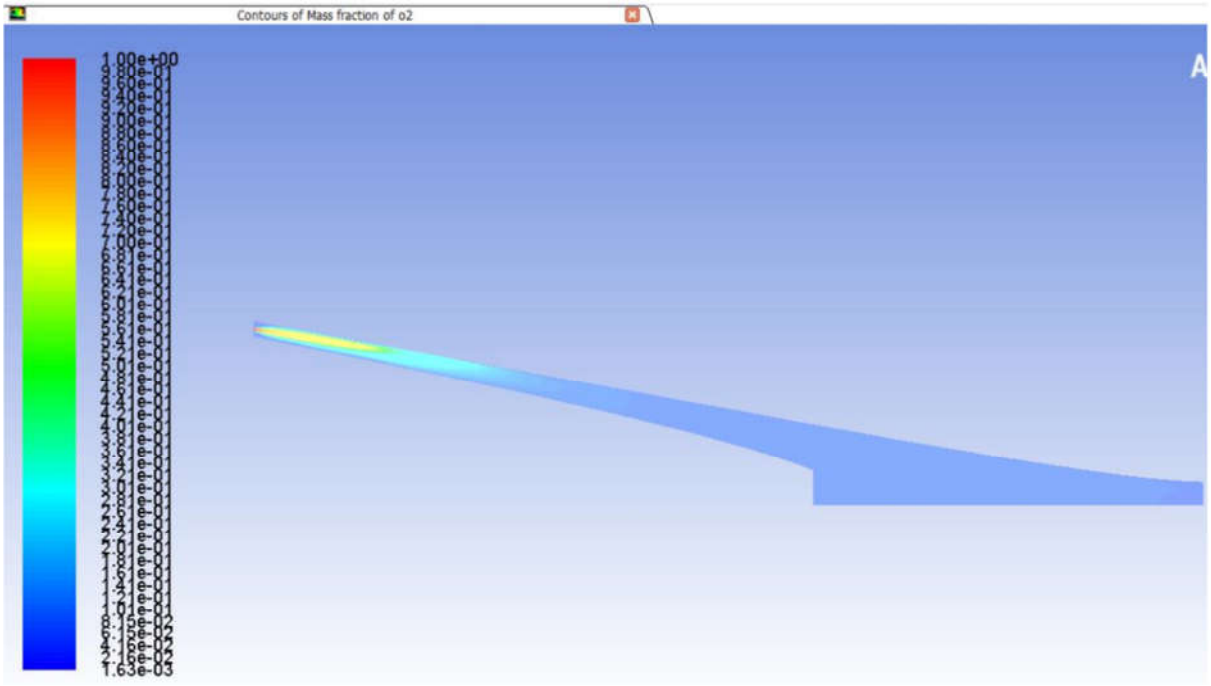

FIG. 23: Contours of oxygen mass fraction.

8. STRUCTURAL DEMONSTRATOR-DESIGN

For the structural design of a hyperboloid gas generator combustion chamber, focusing a 35 kN LOX/LCH4 rocket propulsion system, special features of the design are taken into account. The outer combustion chamber wall is made out of the latest fiber reinforced composites (carbon fiber reinforced plastics – CFRP and CMCs). Firstly the wall-thickness was approximated by using Barlow's formula Eqs. (10) and 11).

$$\sigma_t = \frac{p_{ch} \cdot d_m}{2 \cdot s} \tag{10}$$

$$\sigma_s = \frac{p_{ch} \cdot d_m}{4 \cdot s} \tag{11}$$

$\sigma_t - tangential\ stress$ $\sigma_a - axial\ stress$

$d_m - average\ diameter$ $p_{ch} - chamber\ pressure$

$s - wall\ thickness$

For constant pressure loss between combustion chamber and fuel supply channel, a constant wall thickness of the porous CMC was chosen (Fig. 24). The injection of the fuel occurs completely through the porous CMC walls. For this purpose, the oxidant will be injected only through the face-plate of the injector head, which is designed in cone-injector shape (Fig. 3).

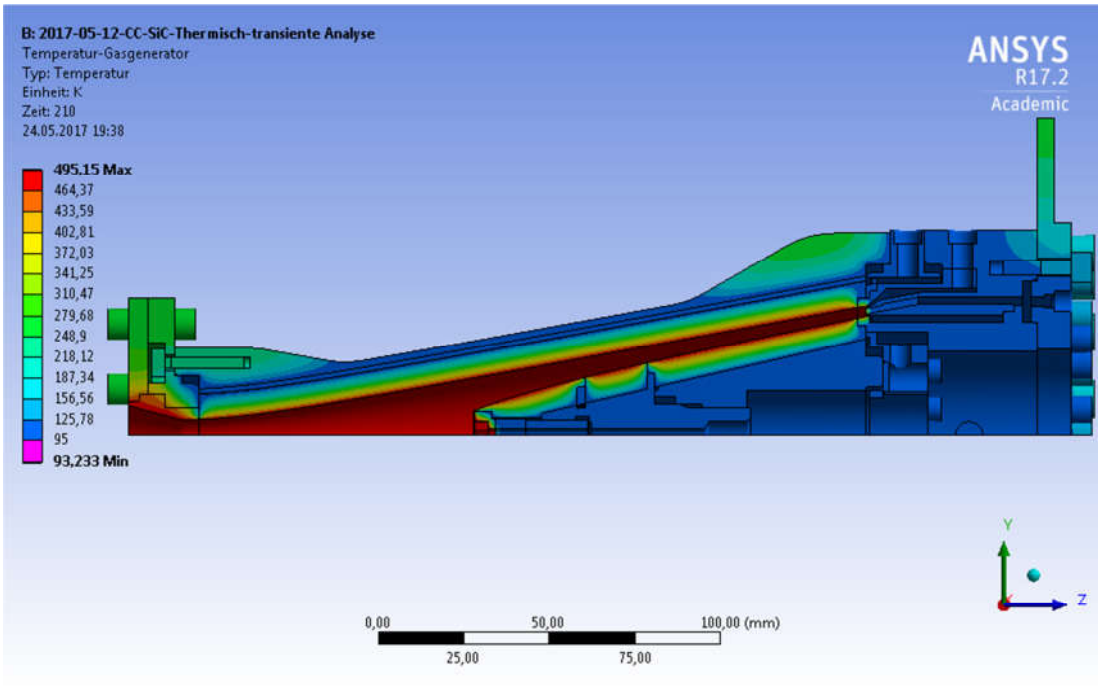

FIG. 24: Temperature distribution of the dual-shell hyperboloid demonstrator, operating in gas generator mode.

For a better fuel processing, two rows of notches for additional film cooling initiation at the face-plate are implemented close to the oxidant injector element. These films provide an additional mixing mechanism and in case of occurring hot spots essential wall protection. All other ceramic parts are operated at non-critical temperature by the use of fuel transpiration cooling. The outer CMC body and the distributor sleeve are placed inside the CFRP housing. The connection between

injector and nozzle will be done the bolt interface (Ortelt 2012). For the fixation of the inner CMC body an individual screw made of INCONEL ® 78 provides the full functionality of the inner core. Caused by a save operation considering a variety of thermo-mechanic load scenarios due to different test objectives (particularly the subscale-case for the main combustion chamber application and its higher overall load level), the pre-cooling phase will be extraordinary long, to prevent structural failure in any case. Considering larger up-scaling geometry for the main chamber application this requirement will be significantly relaxed.

9. OPTICAL SENSORS ON TRANSPIRATION OPERATED SURFACES AND OPTICAL DIAGNOSTICS ON COMBUSTION

During the phase of basic investigations on transpiration cooling in CMC rocket thrust chambers, one major question was the measurement of inner wall surface temperatures. Therefore, the Institute of Space Systems at the University of Stuttgart contributed optical measurement by the use of its PYREX system, a one-color pyrometer operated with its own algorithm for data recording and sampling. Both the miniaturization level and the analogue design helped significantly in the assessment. The former is derived from in-flight investigations for reentry capsules to assess the wall temperatures of the ceramic based heat shield materials. This in turn provides PYREX with a significant heritage e.g. for a later preparation of the system as a health monitoring system for later flight campaigns with ceramic combustion chambers. The latter aspect i.e. the analogue design helps for the detection rate as the sensor system can be read out very quickly allowing for aspects that need a high temporal resolution to be assessed. One example is the switch on and switch off of the chamber as this allows for the identification of remaining combustion radiation contributing to the PYREX system.

In an analyses in which the expected wall temperatures and the spectral radiation properties of the combustion were assessed in a combined way the wavelength 850 nm was identified as an adequate compromise as detection wavelength. The latter has been assessed using a transparent combustion chamber together with an IRS mini spectrometer. A self-developed tool that emulates the signal chain at the whole was then used to simulate the presumable calibration curves of the miniaturized pyrometer.

The system has then been applied in micro-combustor chambers with 30 mm diameter and 10 bar chamber pressure. The O2-H2 mixture ratio amounted to 6.5.

The hardware setup is given in figure 25. The PYREX system was fixed by a thread at a single CMC ring segment component inside a standard copper chamber setup at a downstream position of completely formed combustion (Ortelt 2017).

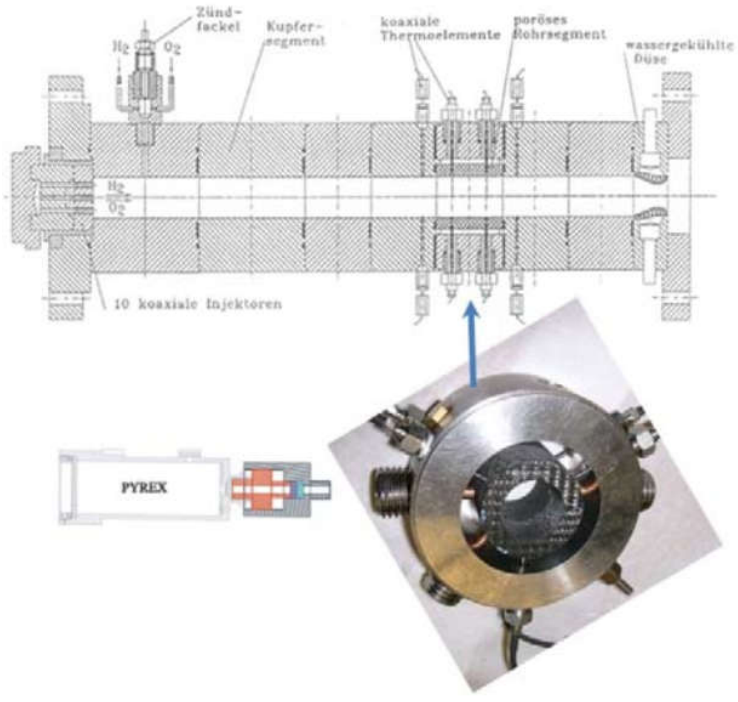

FIG. 25: Potential hardware setup for optical diagnostics.

10. SUMMARY AND OUTLOOK

The new hyperboloid design approach for inner combustion chamber contours in injection-cooled rocket engines shows from several points of view interesting perspectives. On the one hand the potential for the increase of engine efficiency can be seen, because the combination of cooling and injection leads to significant reduction of pressure loss compared to standard cooling methods. On the other hand higher reliability can be expected because of higher blow rates at the inner wall surfaces. Firstly the higher blow rate represents an increase of wall protection and secondly it leads to lifetime increase. Additionally the implementation of health monitoring systems can be realized more easily and with lower risk of damage. First analytical screenings prove at the moment these expectations.

Embedded in a completely load-decoupled structure system as represented by DLR's traditional transpiration cooled ceramic TCA, the new approach promises the potential of long-life engines at reasonable price level, as can be seen in established aviation systems.

In near future projects the described properties and effects will be investigated more detailed, both in experimental work as well as in further theoretical research.

REFERENCES

Greuel, D., (2013). Untersuchungen zum Impuls- und Stofftransport in effusiv gekühlten faserkeramischen Raketenbrennkammerwänden. Dissertation, RWTH Aachen, Germany.

Haidn, O.J., Greuel, D., Ghadjani, S., Ortelt, M., Hald, H., (2003) Application of Fiber Reinforced C/C Ceramic Structures in Liquid Rocket Engines, International Conference (SPACE'2003) "Space Challenge in 21 Century. 100 Years After the Tsiolkokiy Idea on Space Missions Using Reactive Motors", 15-19 September, Moscow – Kaluga, Russia.

Hald, H, Ortelt, M., Fischer, I., Greuel, D., Haidn, O.J., (2005), Effusion Cooled CMC Rocket Combustion Chamber, AIAA/CIRA 13th International Space Planes and Hypersonic Systems Conference, Capua, Italy.

Ortelt, M., Hald, H., Herbertz, A., (2009), Investigations on Fiber Reinforced Combustion Chamber Structures under Effusion Cooled LOX/LH2 Operation, 45th Joint Propulsion Conference, Denver, Colorado.

Herbertz, A., Ortelt, M., Mueller, I., Hald, H., (2012), Transpiration cooled Ceramic Thrust Chamber Applicability for High-Thrust Rocket Engines, 48th AAIA/ASME/SAE/ASEE Joint Propulsion Conference, 30 Jul – 1 Aug, Atlanta, Georgia.

Herbertz, A., Selzer, M., (2012), Systems Analysisi of a LOX/LH2 Rocket Engine with a Transpiration-Cooled Ceramic Thrust-Chamber, 48th AAIA/ASME/SAE/ASEE Joint Propulsion Conference, 30 Jul – 1 Aug, Atlanta, Georgia.

Michaelides, S., (2016), Ansys-CFX-Simulation einer keramischen Gasgenerator-Brennkammer fuer einen LOX/LCH4 Raketenantrieb der 35 kN Klasse, Grosser Beleg (Internal Report) ILR-RFS GB 16-07, Technical University of Dresden, Germany.

Michaelides, S., (2017), Systematische und numerische Betrachtung von Treibstoffaufbereitung

und Verbrennung in einem neuartigen Injektor-Brennkammer-Konzept fuer Raumfahrtantriebe, Diplomarbeit (Internal Report) ILR-RFS DA 17-06, Technical University of Dresden, Germany.

Ortelt, M., Hald, H., Herbertz, A., Mueller, I., (2013), Advanced Design Concepts for Ceramic Thrust Chamber Components of Rocket Engines, 5th EUROPEAN CONFERENCE FOR AERONAUTICS AND SPACE SCIENCES (EUCASS), Munich, Germany.

Ortelt, M., Hald, H., Herbertz, A., Rotaermel, W., (2010), CMC Design Approach for Cryogenic Injector Heads of Rocket Thrust Chambers, European Conference on Materials and Structures in Aerospace, 07 – 08 June, Berlin, Germany.

Ortelt, M., Elsaesser, H., Herbertz, A., Mueller, I., Hald, H., (2012), Structural Investigations on Cryogenically Operated and Transpiration Cooled Fiber Reinforced Rocket Thrust Chambers, 48th AAIA/ASME/SAE/ASEE Joint Propulsion Conference, 30 Jul – 1 Aug, Atlanta, Georgia.

Ortelt, M., Hald, H., Mueller, I., (2014), Status and Future Perspectives of the CMC Rocket Thrust Chamber Development at DLR, 65th International Astronautical Congress IAC, Toronto, Canada.

Ortelt, M., Hald, H., Michaelides, S., Seiler, H., Herdrich, G., (2017), Advancement of Rocket Engine Performance through Novel Approaches for Thrust Chamber Design, 68th International Astronautical Congress IAC, Adelaide, Australia.

Schleutker, T., (2014), Analytischer und numerischer Vergleich des Wandwaermestroms bei konventionellen und hyperbolischen Brennkammern, Diplomarbeit (Internal Report), Institute of Space Systems at the Technical University of Stuttgart and Institute of Structures and Design at DLR Stuttgart, Germany.

Seiler, H., (2017), Structural design of the hyperboloid gas generator combustion chamber for a

35 kN LOX/Methane rocket propulsion system, master thesis (Internal Report) IRS-17-S048, University of Stuttgart, Germany.

Selzer, M., Schweikert, S., Hald, H., Wolfersdorf, J. von, (2013), Transfer of analytical transpiration cooling model to the cooling analysis of rocket combustion chambers made of ceramic matrix composites, 5th EUROPEAN CONFERENCE FOR AERONAUTICS AND SPACE SCIENCES (EUCASS), Munich, Germany.

Weuta, P., Jaschinski, N., (2016), Low Cost Propulsion Systems for Launch-, In Space- and Space Tourism Applications, Space Propulsion Conference, Rome, Italy.

Chehroudi, B., Davis, D., Talley, D., (2002), Cryogenic shear layers: experiments and phenomenological modeling of the initial growth rate under subcritical and supercritical conditions. In: International Journal of Heat and Fluid Flow 23.

Peters, N., (2010), Technische Verbrennung, Vorlesungsskript, Institut fuer Technische Verbrennung, RWTH, Aachen, Germany.

Thring, M., Mewby, M., (1953) Combustion length of enclosed turbulent jet flames. 4. Symp. Combustion, Baltimore.

ANSYS Fluent Theory Guide 17.1, (2016).